

# Spatial and spectral analysis of occluded motions

Cicero Mota <sup>a,1</sup>, Ingo Stuke <sup>b</sup>, Til Aach <sup>b</sup>, and Erhardt Barth <sup>a</sup>

<sup>a</sup>*Institute for Neuro- and Bioinformatics*

<sup>b</sup>*Institute for Signal Processing*

*University of Lübeck, Ratzeburger Allee 160, 23538 Lübeck, Germany*

---

## Abstract

We present a spatio-temporal analysis of motion at occluding boundaries. The main result is an analytical description of the motions and the distortions that occur at the occluding boundary. Based on this result we analyze occluding motions in the Fourier domain and show that the distortion term has an hyperbolic decay independent of the shape of the occluding boundary. Moreover, we derive the exact expression for the distortion term for the case of straight boundaries. The results are illustrated by using simulations with synthetic movies.

---

## 1 Introduction

Motion estimation is essential in a variety of image processing and computer vision tasks, like video coding, tracking, directional filtering and denoising, scene analysis, etc. Accordingly, motion estimation is still a major subject of research interest for the image processing community. Especially, the accurate estimation of motion at occluding boundaries remains a challenging problem. Proposed techniques include adaptive regularization [1], superposition models [2], distributed representations [3], multiple-frame integration [4], spectral analysis [5–7], image and motion mixture models [8], and robust estimation methods [9,10]. Nevertheless, a satisfactory technique has not yet been developed due to a lack of theoretical understanding [11]. One way to better understand occluded motions is to analyze how exactly superposition models [2,6] fail at occlusions. We here derive a new spatial constraint for the distortions induced by the occluding boundary and analyze the result in the

---

<sup>1</sup> CM is also affiliated with the University of Amazonas, Brazil.

Fourier domain. The results are based on earlier work on transparent and occluded motions [12–15]. The model of occlusion that we use is due to Fleet and Langley [5] who also analyzed occluded motions in the Fourier domain. This type of analysis was further developed in [7,11]. Alternative spatial approaches have been developed in [3,4]. Before presenting the new results in the spatial and Fourier domain, we will briefly review the problem of motion estimation by pointing out the transitions needed from single to transparent and finally occluded motions.

### 1.1 Single motion

We represent an image sequence by a function  $f(\mathbf{x}, t)$ , where  $\mathbf{x} = (x, y)$  and  $t$  are the space and time variables. Under the hypothesis that image intensity changes only due to motion, the well-known Brightness Constancy Constraint Equation (BCCE) applies [16]:

$$\frac{df}{dt} = v_x f_x + v_y f_y + f_t = 0, \quad (1)$$

where  $\mathbf{v} = (v_x, v_y)$  is the velocity and  $f_x, f_y, f_t$  denote the partial derivatives of  $f$ . Different methods have been proposed to estimate the motion field by using Equation (1). A review of available methods can be found in [17].

### 1.2 Transparent motions

Equation (1) has been extended for the case of multiple transparent motions by Shizawa and Mase [18,2]. They model transparent motions as the superposition

$$f(\mathbf{x}, t) = g_1(\mathbf{x}, t) + g_2(\mathbf{x}, t) \quad (2)$$

of two image sequences. Under the assumption of locally constant motions, the layers can be modeled as  $g_1(\mathbf{x}, t) = g_1(\mathbf{x} - t\mathbf{u})$  and  $g_2(\mathbf{x}, t) = g_2(\mathbf{x} - t\mathbf{v})$  both moving with constant velocities  $\mathbf{u}$  and  $\mathbf{v}$  respectively. Let the operator  $\alpha(\mathbf{u}) = u_x \frac{\partial}{\partial x} + u_y \frac{\partial}{\partial y} + \frac{\partial}{\partial t}$  denote the derivative along  $\mathbf{u} + \mathbf{e}_t$ , where  $\mathbf{e}_t$  represents the time axis. The operator  $\alpha(\mathbf{v})$  is defined in a similar way. Under the above hypothesis,  $\alpha(\mathbf{u}), \alpha(\mathbf{v})$  commute and therefore

$$\alpha(\mathbf{u})\alpha(\mathbf{v})f(\mathbf{x}, t) = 0. \quad (3)$$

### 1.3 Occluded motions

Let us suppose that a foreground object moves with constant velocity  $\mathbf{u}$  and the background moves with constant velocity  $\mathbf{v}$ . The image sequence can be modeled by [5]

$$f(\mathbf{x}, t) = \chi(\mathbf{x} - t\mathbf{u})g_1(\mathbf{x} - t\mathbf{u}) + [1 - \chi(\mathbf{x} - t\mathbf{u})]g_2(\mathbf{x} - t\mathbf{v}). \quad (4)$$

where

$$\chi(\mathbf{x}) = \begin{cases} 1 & \text{if } \mathbf{x} \in \Omega \\ 0 & \text{otherwise} \end{cases} \quad (5)$$

and  $\Omega$  is the support of the foreground object.

Since the motion constraint  $\alpha(\mathbf{u})f(\mathbf{x}, t) = 0$  is valid in the interior of  $\Omega$  and the constraint  $\alpha(\mathbf{v})f(\mathbf{x}, t) = 0$  is valid in the exterior of  $\Omega$ , the constraint  $\alpha(\mathbf{u})\alpha(\mathbf{v})f(\mathbf{x}, t) = 0$  is valid everywhere but at the occluding boundary. We therefore analyze the distortion induced by the occluding boundary, i.e. the residual of the superposition constraint.

## 2 Spatial analysis of motion at occluding boundaries

We apply the operator  $\alpha(\mathbf{u})\alpha(\mathbf{v})$  to the motion model at the occluding boundary under the hypothesis of ‘locally constant motions’.

By applying the operator  $\alpha(\mathbf{u})$  to Equation (4), we obtain

$$\alpha(\mathbf{u})f(\mathbf{x}, t) = [1 - \chi(\mathbf{x} - t\mathbf{u})]\alpha(\mathbf{u})[g_2(\mathbf{x} - t\mathbf{v})]. \quad (6)$$

$\alpha(\mathbf{u})[g_2(\mathbf{x} - t\mathbf{v})]$  in the above equation simplifies to  $(\mathbf{u} - \mathbf{v}) \cdot \nabla g_2(\mathbf{x} - t\mathbf{v})$ . Therefore,

$$\alpha(\mathbf{u})\alpha(\mathbf{v})f(\mathbf{x}, t) = -\alpha(\mathbf{v})[\chi(\mathbf{x} - t\mathbf{u})](\mathbf{u} - \mathbf{v}) \cdot \nabla g_2(\mathbf{x} - t\mathbf{v}). \quad (7)$$

The derivatives of the discontinuous mask  $\chi$  need to be taken in the sense of distribution theory [19]. In Appendix A, we show that

$$\alpha(\mathbf{v})[\chi(\mathbf{x} - t\mathbf{u})] = (\mathbf{u} - \mathbf{v}) \cdot \mathbf{N}(\mathbf{x} - t\mathbf{u})\delta(B(\mathbf{x} - t\mathbf{u})) \quad (8)$$

where  $B(\mathbf{x}) = 0$  determines the boundary of  $\Omega$  and  $\mathbf{N}(\mathbf{x}) = \nabla B(\mathbf{x})$  is the unit normal to the boundary. We have therefore proven the following

**Proposition 1** *If an image sequence is given by Equation (4) then*

$$\alpha(\mathbf{u})\alpha(\mathbf{v})f(\mathbf{x}, t) = q(\mathbf{x}, t, \mathbf{u}, \mathbf{v})\delta(B(\mathbf{x} - t\mathbf{u})), \quad (9)$$

where

$$q(\mathbf{x}, t, \mathbf{u}, \mathbf{v}) = -(\mathbf{u} - \mathbf{v}) \cdot \mathbf{N}(\mathbf{x} - t\mathbf{u}) (\mathbf{u} - \mathbf{v}) \cdot \nabla g_2(\mathbf{x} - t\mathbf{v}). \quad (10)$$

Equation (9) has a simple intuitive meaning:  $\alpha(\mathbf{u})\alpha(\mathbf{v})f(\mathbf{x}, t)$  vanishes almost everywhere but at the occluding boundary where it becomes a Dirac distribution due to the discontinuity at the boundary of the mask  $\chi$ . Thus, motion estimation fails at occlusions because both Equations (1) and (3) are not valid at points on the occluding boundary. The valid equation is Equation (9). To estimate two occluding motions we can therefore either use Equation (3) but do not integrate at occlusion points where we have motion discontinuities [14,15], or solve Equation (9) to perform the estimation.

Moreover, there are a few conclusions to be drawn from Equations (9) and (10): the distortion is (i) restricted to the occluding boundary, (ii) minimal when the normal to the boundary is orthogonal to the relative motion (the difference between fore- and background motions) and maximal when the two vectors are aligned, (iii) proportional to the intensity gradient of the background pattern. Some of these relationships are illustrated in the Fourier domain by Figures 2 to 4.

### 3 Fourier analysis of motion at occluding boundaries

The Fourier-domain analysis of motion is known to be intuitive and has led to novel methods, e.g., based on the observation that a single motion corresponds to a plane. The Fourier analysis of occluded motions, however, has so far been restricted to the case of straight image boundaries. We shall here overcome this restriction by using the result of the previous section. In the following we represent by capital letters the Fourier transform of the corresponding signal, e.g.,  $F$  is the Fourier transform of  $f$ .

To simplify notation, we set

$$h(\mathbf{x}) = -(\mathbf{u} - \mathbf{v}) \cdot \mathbf{N}(\mathbf{x})\delta(B(\mathbf{x})). \quad (11)$$

With this notation, the residual in the right-hand side of Equation (9) becomes

$$r(\mathbf{x}, t) = (\mathbf{u} - \mathbf{v}) \cdot \nabla g_2(\mathbf{x} - t\mathbf{v})h(\mathbf{x} - t\mathbf{u}) \quad (12)$$

and in the Fourier domain

$$R(\boldsymbol{\xi}, \xi_t) = 2\pi j [(\mathbf{u} - \mathbf{v}) \cdot \boldsymbol{\xi} G_2(\boldsymbol{\xi})\delta(\mathbf{v} \cdot \boldsymbol{\xi} + \xi_t)] * [H(\boldsymbol{\xi})\delta(\mathbf{u} \cdot \boldsymbol{\xi} + \xi_t)]. \quad (13)$$

The expansion of the above convolution involves the integration of

$$\delta(\mathbf{v} \cdot \boldsymbol{\omega} + \omega_t) \delta(\mathbf{u} \cdot \boldsymbol{\xi} + \xi_t - \mathbf{u} \cdot \boldsymbol{\omega} - \omega_t) \quad (14)$$

in the variables  $\boldsymbol{\omega}, \omega_t$ . That is, we have to integrate a  $\delta$ -line with support  $L$  defined by the solution of

$$\begin{aligned} \mathbf{v} \cdot \boldsymbol{\omega} + \omega_t &= 0 \\ \mathbf{u} \cdot \boldsymbol{\omega} + \omega_t &= \mathbf{u} \cdot \boldsymbol{\xi} + \xi_t. \end{aligned} \quad (15)$$

The cross section of this  $\delta$ -line is  $d = |(\mathbf{u} + \mathbf{e}_t) \times (\mathbf{v} + \mathbf{e}_t)|^{-1}$  (see [20]). Note that  $(\mathbf{u} - \mathbf{v}) \cdot \boldsymbol{\omega} = \mathbf{u} \cdot \boldsymbol{\xi} + \xi_t$  and thus factors out of the integral. Therefore,

$$R(\boldsymbol{\xi}, \xi_t) = 2d\pi j(\mathbf{u} \cdot \boldsymbol{\xi} + \xi_t) \int_L G_2(\boldsymbol{\omega}) H(\boldsymbol{\xi} - \boldsymbol{\omega}) ds, \quad (16)$$

where  $s$  is the arc-length of  $L$ . We have therefore proven the following

**Proposition 2** *The spectrum of  $f(\mathbf{x}, t)$  is given by*

$$F(\boldsymbol{\xi}, \xi_t) = A(\boldsymbol{\xi})\delta(\mathbf{u} \cdot \boldsymbol{\xi} + \xi_t) + B(\boldsymbol{\xi})\delta(\mathbf{v} \cdot \boldsymbol{\xi} + \xi_t) + C(\boldsymbol{\xi}, \xi_t) \quad (17)$$

where

$$C(\boldsymbol{\xi}, \xi_t) = \frac{d}{2\pi j(\mathbf{v} \cdot \boldsymbol{\xi} + \xi_t)} \int_L G_2(\boldsymbol{\omega}) H(\boldsymbol{\xi} - \boldsymbol{\omega}) ds. \quad (18)$$

The first two components of the sum in Equation (17) are the two motion planes and the third component defined by Equation (18) is the distortion term.

Note that the shape of the distortion term is determined by the hyperbolic decay, as long as  $H(\boldsymbol{\omega})$  is limited, because the support  $L$  of the integral does not change if  $\boldsymbol{\xi} + \xi_t \mathbf{e}_t$  belongs to the plane  $\mathbf{u} \cdot \boldsymbol{\xi} + \xi_t = c$ . For any practical purpose it is safe to assume  $H(\boldsymbol{\omega})$  since

$$|H(\boldsymbol{\omega})| \leq |\mathbf{u} - \mathbf{v}| \text{length}(B). \quad (19)$$

The spectrum of occlusion has been analyzed by Beauchemin *et al.* under the assumption of a straight boundary [21,22,7,11,23]. They found that, in this case,

$$\begin{aligned} A(\boldsymbol{\xi}) &= \left[ \pi \delta(\boldsymbol{\xi}) + \frac{1}{j\mathbf{N} \cdot \boldsymbol{\xi}} \delta(\mathbf{N}^\perp \cdot \boldsymbol{\xi}) \right] * G_1(\boldsymbol{\xi}) \\ B(\boldsymbol{\xi}) &= (1 - \pi) G_2(\boldsymbol{\xi}), \end{aligned} \quad (20)$$

where  $\mathbf{N}^\perp$  is a unity vector normal to  $\mathbf{N}$ . They also recognized the hyperbolic decay of  $C(\boldsymbol{\xi}, \xi_t)$  but the exact expression of the distortion remained unspecified. We will now use the above results to determine  $C(\boldsymbol{\xi}, \xi_t)$ . If the support

$\Omega$  of the occluding signal is a half-plane, the border of occlusion is the line  $B(\mathbf{x}) = \mathbf{N} \cdot \mathbf{x} = 0$  and we can evaluate the integral in Equation (18). In this case, we have

$$h(\mathbf{x}) = -(\mathbf{u} - \mathbf{v}) \cdot \mathbf{N} \delta(\mathbf{N} \cdot \mathbf{x}) \quad (21)$$

and in the Fourier domain

$$H(\boldsymbol{\xi}) = -(\mathbf{u} - \mathbf{v}) \cdot \mathbf{N} \delta(\mathbf{N}^\perp \cdot \boldsymbol{\xi}). \quad (22)$$

Replacement of  $H(\boldsymbol{\xi})$  in Equation (18) (or directly in Equation (13)) gives us

$$C(\boldsymbol{\xi}, \xi_t) = \frac{\text{sign}((\mathbf{u} - \mathbf{v}) \cdot \mathbf{N})}{2\pi j(\mathbf{v} \cdot \boldsymbol{\xi} + \xi_t)} G_2(\boldsymbol{\omega}) \quad (23)$$

where

$$\boldsymbol{\omega} = \boldsymbol{\omega}(\boldsymbol{\xi}, \xi_t) = \frac{(\mathbf{u} \cdot \boldsymbol{\xi} + \xi_t)\mathbf{N} + \boldsymbol{\xi} \cdot \mathbf{N}^\perp(\mathbf{u} - \mathbf{v})^\perp}{(\mathbf{u} - \mathbf{v}) \cdot \mathbf{N}}. \quad (24)$$

Therefore, it is straightforward to conclude that the profile of the distortion function is hyperbolic along lines with orientation  $\mathbf{N} - \mathbf{u} \cdot \mathbf{N}\mathbf{e}_t$  because along such lines  $\boldsymbol{\omega}(\boldsymbol{\xi}, \xi_t)$  is constant; and has the same profile as the occluded signal along the planes  $\mathbf{v} \cdot \boldsymbol{\xi} + \xi_t = c$ .

## 4 Experimental results

The experimental results are based on synthetic imagery and are meant to illustrate the above theoretical results. We use noise patterns for both the foreground and the background. The shapes of foreground and background are shown in Figure 1. The radius of the small circle was 30 pixels and of the large circle 128 pixels. Both foreground and background move and the directions of motion are indicated in the captions of Figures 2 and 3. In addition, noise (SNR 30 dB) was added to the resulting movies such as to view the spectral structures relative to this realistic noise level. The movies are 128 pixels large in all three directions and have been windowed with a Hanning window such that the shown spectra visualize local properties of the movies. In all figures the residual is depicted by subtracting the spectra of occlusion and transparency. Accordingly to Equation 18 the most blurred plane corresponds to the spectrum of occlusion. This is clearly seen in Figures 2 (c); 3 (b) and (c); and 4 (b), (c) and (f). For better visualization, the amplitude spectrum is shown after taking the logarithm.

Figure 2 shows results obtained for a straight occluding boundary - see Figure 1 (a). By comparison of (a) and (b) we note that, according to Equation (10), transparent and occluded motions are equivalent if the motions of the occluding layers are such that the distortion term is zero (relative motion

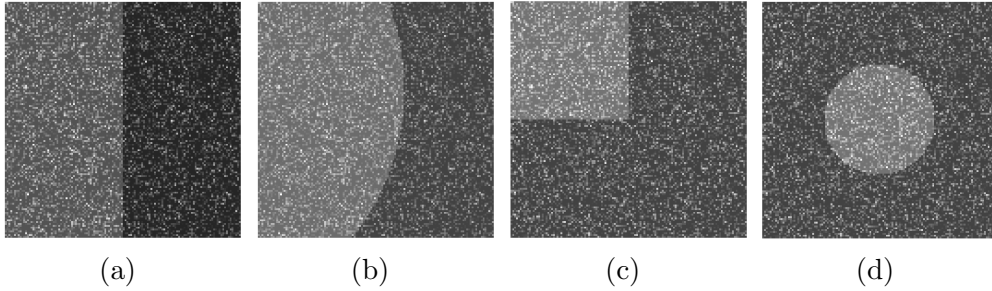


Fig. 1. The shape of different objects with noisy texture moving in front of a noisy background. Superposition is either transparent or occluding.

perpendicular to the boundary normal). Panel (c) shows, again for a straight boundary, the maximum distortion (the relative motion is perpendicular to the boundary). Panel (d) show the distortion due to occlusion, i.e., the difference between (c) and (a).

Figure 3 shows results analogous to those in Figure 2 (b), (c) and (d) but for curved boundaries - see Figure 1 (b). Note in panel (b) that the curvature of the boundary induces a distortion not present in panel (b) of Figure 2. Also note that the distortion is increased when the relative motion direction is approximately perpendicular to the boundary - see panel (c). The distortion due to occlusion is shown in panel (d). No substantial difference is observable between the maximal distortion for curved and straight boundaries - compare Figure 2 (d) against 3 (d).

Figure 4 show results for highly curved boundaries. It demonstrates that 2D features like dots and corners are good features to track even in the case of occluded motions - see Figure 1 (c) and (d). For the corner, the distortion is less than for straight boundaries and it varies less with the directions of motion, compare against Figure 2 (c) and Figure 3 (c). panels (b) and (c). For the small circle in (f) the distortion obviously does not depend on the directions of motions relative to the normal since the normals point in all directions. The distortion due to occlusion are shown in panels (d) and (g) for the corner and small circle respectively.

## 5 Discussion

Although the problem of estimating motion at occluding boundaries has already been studied extensively, we have here added an important missing part, which is an equation that describes motion at the occluding boundary including the expression for the distortion term given both in the spatial and the Fourier domains.

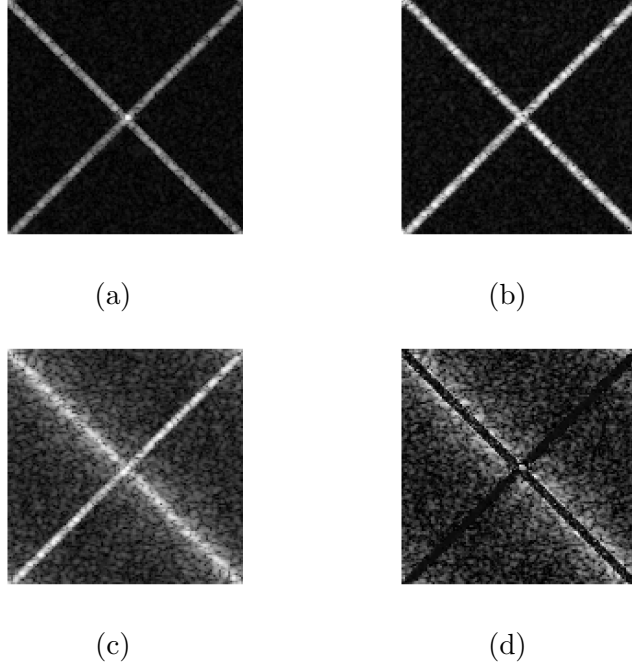


Fig. 2. Straight boundaries. Shown are the amplitude spectra ( $\xi_t = 64$ ) of (a) a transparent sequence with velocities  $\mathbf{u} = (1, 1)$  and  $\mathbf{v} = (-1, 1)$ ; (b) an occlusion sequence with straight boundary and velocities  $\mathbf{u} = (1, 1)$  and  $\mathbf{v} = (1, -1)$  for the foreground and background respectively; (c) an occlusion sequence with straight boundary and velocities  $\mathbf{u} = (1, 1)$  and  $\mathbf{v} = (-1, 1)$ ; (d) the difference between (c) and (a). Note how the distortion due to the occlusion depends on the relative motion and the normal to the boundary: no distortion in (b), maximal distortion in (c). In (d) we can clearly see the hyperbolic decay of the distortion term.

By our spatial analysis we have been able to show precisely what distortions are to be expected when algorithms based on superposition models are used to estimate motion at occlusions. This result is the basis for the subsequent Fourier analysis.

Fourier analysis has revealed that the decay of the distortion is hyperbolic for both straight and curved boundaries. Previously this result had been validated only for straight boundaries [21,22,7,11,23]. Moreover, we have determined the exact expression for the distortion term for the case of straight boundaries.

Our synthetic examples illustrate the results by showing that (i) both transparent and occluded motions lie in two planes if the relative motions are orthogonal to the normal of the occluding boundary, (ii) the distortion is similar in shape for straight and curved boundaries and somewhat smaller for curved boundaries because the normal changes within the integration region, (iii) motion estimation is more reliable at corners and curved boundaries due to a smaller distortion term.

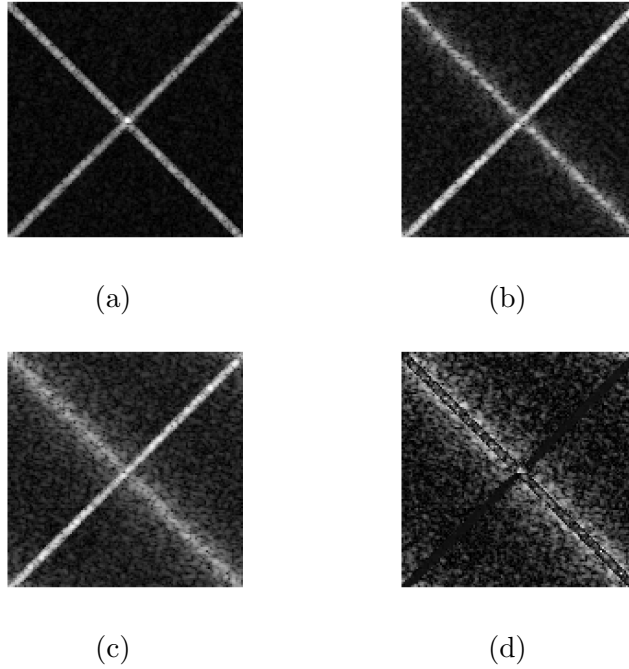


Fig. 3. Curved boundaries. Shown are the amplitude spectra ( $\xi_t = 64$ ) of (a) a transparent sequence with a large circular foreground object that moves with velocity  $\mathbf{u} = (1, 1)$  over a background that moves with  $\mathbf{v} = (1, -1)$ ; (b) same as in (a) but occlusion. (c) same as in (b) but velocity  $\mathbf{v} = (-1, 1)$ ; (d) the difference between (c) and (a). Maximal and minimal distortion is again observable.

We conclude that the performance of algorithms based on either superposition models or the estimation of motion planes in the Fourier domain will be largely affected by the direction of the relative motion and the orientation of the boundary. In the particular but frequent case of stationary backgrounds, the distortion term depends only on the direction of motion relative to the orientation of the occluding boundary.

### Acknowledgements

This work has been supported by the DFG under Ba 1176/7-2. We thank the reviewers for valuable suggestions.

### References

- [1] E. C. Hildreth, The computation of the velocity field, Proceedings of the Royal Society of London B 221 (1984) 189-220.

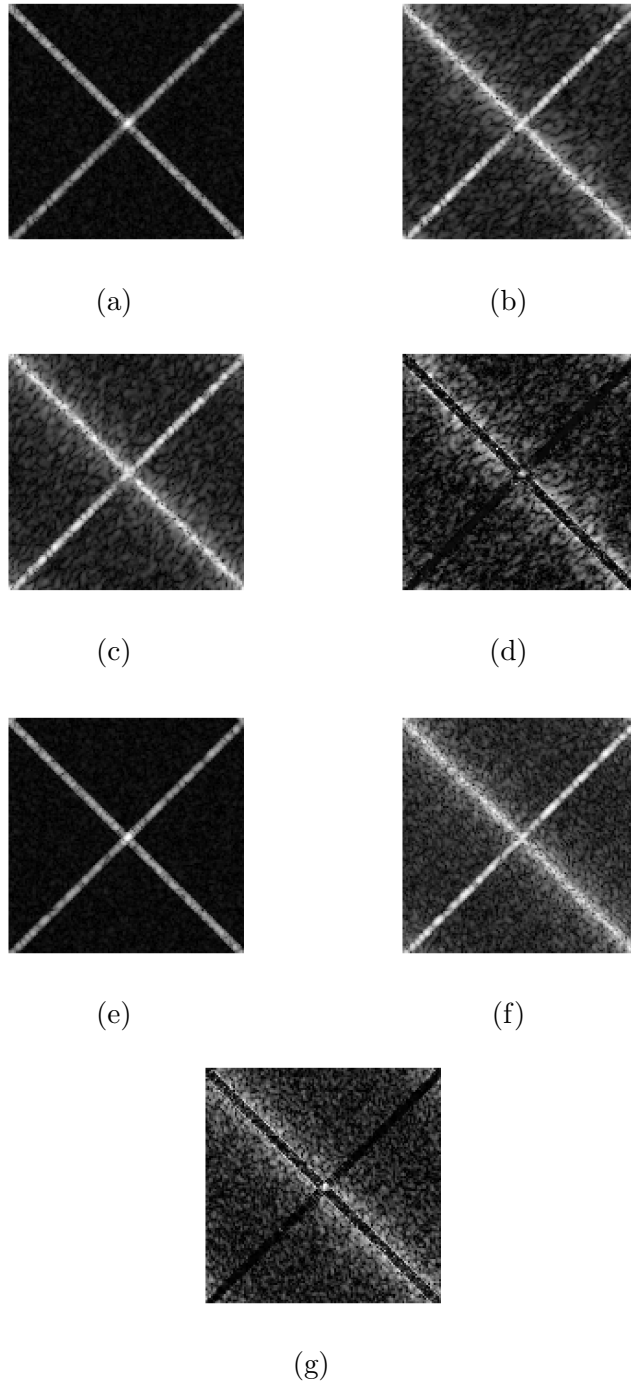


Fig. 4. Good features to track. Shown are the amplitude spectra ( $\xi_t = 64$ ) of (a) a transparent sequence with a corner-shaped object as foreground, and velocities  $\mathbf{u} = (1, 1)$  and  $\mathbf{v} = (1, -1)$ ; (b) same as in (a) but occlusion; (c) same as in (b) but velocities  $\mathbf{u} = (1, 1)$  and  $\mathbf{v} = (-1, 1)$ ; (d) the difference between (c) and (a); (e) a transparent sequence with a small circular foreground object and velocities  $\mathbf{u} = (1, 1)$  and  $\mathbf{v} = (-1, 1)$ ; (f) same as in (e) but occlusion; and (g) the difference between (f) and (e).

- [2] M. Shizawa, K. Mase, A unified computational theory for motion transparency and motion boundaries based on eigenenergy analysis, in: IEEE Conf. Computer Vision and Pattern Recognition, IEEE Computer Press, Maui, HI, 1991, pp. 289–95.
- [3] T. Darrell, E. Simoncelli, Nulling filters and the separation of transparent motions, in: IEEE Conf. Computer Vision and Pattern Recognition, IEEE Computer Press, New York, 1993, pp. 738–9.
- [4] M. Irani, B. Rousso, S. Peleg, Computing occluding and transparent motions, *International Journal of Computer Vision* 12 (1) (1994) 5–16.
- [5] D. J. Fleet, K. Langley, Computational analysis of non-Fourier motion, *Vision Research* 34 (22) (1994) 3057–79.
- [6] D. Vernon, Decoupling Fourier components of dynamic image sequences: a theory of signal separation, image segmentation and optical flow estimation, in: H. Burkhardt, B. Neumann (Eds.), *Computer Vision - ECCV'98*, Vol. 1407/II of LNCS, Springer Verlag, 1998, pp. 68–85.
- [7] S. S. Beauchemin, J. L. Barron, The frequency structure of 1D occluding image sequences, *IEEE Trans. Pattern Analysis and Machine Intelligence* 22 (2) (2000) 200–6.
- [8] Y. Weiss, E. H. Adelson, A unified mixture framework for motion segmentation: Incorporating spatial coherence and estimating the number of models, in: IEEE Conf. Computer Vision and Pattern Recognition, 1996, pp. 321–6.
- [9] J. Y. A. Wang, E. H. Adelson, Layered representation for motion analysis, in: IEEE Conf. Computer Vision and Pattern Recognition, New York, 1993, pp. 361–6.
- [10] J. Y. A. Wang, E. H. Adelson, Representing moving images with layers, *IEEE Transactions on Image Processing* 3 (5) (1994) 625–38.
- [11] W. Yu, G. Sommer, S. Beauchemin, K. Daniilidis, Oriented structure of the occlusion distortion: is it reliable?, *IEEE Trans. Pattern Analysis and Machine Intelligence* 24 (9) (2002) 1286–90.
- [12] C. Mota, I. Stuke, E. Barth, Analytic solutions for multiple motions, in: Proc. IEEE Int. Conf. Image Processing, Vol. II, IEEE Signal Processing Soc., Thessaloniki, Greece, 2001, pp. 917–20.
- [13] I. Stuke, T. Aach, C. Mota, E. Barth, Estimation of multiple motions: regularization and performance evaluation, in: B. Vasudev, T. R. Hsing, A. G. Tescher, T. Ebrahimi (Eds.), *Image and Video Communications and Processing 2003*, Vol. 5022 of Proceedings of SPIE, 2003, pp. 75–86.
- [14] E. Barth, I. Stuke, C. Mota, Analysis of motion and curvature in image sequences, in: Proc. IEEE Southwest Symp. Image Analysis and Interpretation, IEEE Computer Press, Santa Fe, NM, 2002, pp. 206–10.

- [15] E. Barth, I. Stuke, T. Aach, C. Mota, Spatio-temporal motion estimation for transparency and occlusion, in: Proc. IEEE Int. Conf. Image Processing, Vol. III, IEEE Signal Processing Soc., Barcelona, Spain, 2003, pp. 69–72.
- [16] B. Horn, B. Schunck, Determining optical flow, *Artificial Intelligence* 17 (1–3) (1981) 185–203.
- [17] H. Haußecker, H. Spies, Motion, in: B. Jähne, H. Haußecker, P. Geißler (Eds.), *Handbook of Computer Vision and Applications*, Vol. 2, Academic Press, 1999, pp. 309–96.
- [18] M. Shizawa, K. Mase, Simultaneous multiple optical flow estimation, in: IEEE Conf. Computer Vision and Pattern Recognition, Vol. I, IEEE Computer Press, Atlantic City, NJ, 1990, pp. 274–8.
- [19] F. G. Friedlander, M. Joshi, *Introduction to the Theory of Distributions*, 2nd Edition, Cambridge University Press, 1999.
- [20] R. Bamler, *Mehrdimensionale lineare Systeme*, Springer-Verlag, 1989.
- [21] S. S. Beauchemin, K. Daniilidis, R. Bajcsy, Computing multiple image motions, in: *Vision Interface 99*, 1999, pp. 544–51.
- [22] W. Yu, K. Daniilidis, S. Beauchemin, G. Sommer, Detection and characterization of multiple motion points, in: IEEE Conf. Computer Vision and Pattern Recognition, Vol. I, IEEE Computer Press, Fort Collins, CO, 1999, pp. 171–7.
- [23] W. Yu, G. Sommer, K. Daniilidis, Multiple motions analysis: in spatial or in spectral domain?, *Computer Vision and Image Understanding* 90 (2) (2003) 129–52.

## A Appendix – Evaluation of $\alpha(\mathbf{v})[\chi(\mathbf{x} - t\mathbf{u})]$

Since the mask  $\chi$  is discontinuous, derivatives must be treated using the theory of distributions, i.e., they are defined by ‘identities’ such as

$$\left\langle \frac{\partial \chi}{\partial x}, \phi \right\rangle = - \int \chi(\mathbf{x}) \frac{\partial \phi}{\partial x}(\mathbf{x}) \, d\mathbf{x}, \quad (\text{A.1})$$

where  $\phi$  is a Schwartz test function, e.g., a smooth function with compact support.

We will first show that

$$-\alpha(\mathbf{v})[\chi(\mathbf{x} - t\mathbf{u})] = (\mathbf{u} - \mathbf{v}) \cdot \nabla \chi(\mathbf{x} - t\mathbf{u}). \quad (\text{A.2})$$

In fact,

$$-\langle \alpha(\mathbf{v})[\chi(\mathbf{x} - t\mathbf{u})], \phi \rangle = \int \chi(\mathbf{x} - t\mathbf{u}) [\mathbf{v} \cdot \nabla \phi(\mathbf{x}, t) + \phi_t(\mathbf{x}, t)] d\mathbf{x} dt. \quad (\text{A.3})$$

By introducing the change of coordinates  $\mathbf{y} = \mathbf{x} - t\mathbf{u}$  and observing that

$$\frac{\partial \phi(\mathbf{y} + t\mathbf{u}, t)}{\partial t} = \mathbf{u} \cdot \nabla \phi(\mathbf{y} + t\mathbf{u}, t) + \phi_t(\mathbf{y} + t\mathbf{u}, t) \quad (\text{A.4})$$

integrates to zero, we obtain

$$\begin{aligned} -\langle \alpha(\mathbf{v})[\chi(\mathbf{x} - t\mathbf{u})], \phi \rangle &= \int \chi(\mathbf{y}) (\mathbf{v} - \mathbf{u}) \cdot \nabla \phi(\mathbf{y} + t\mathbf{u}, t) d\mathbf{y} dt \\ &= \int (\mathbf{u} - \mathbf{v}) \cdot \nabla \chi(\mathbf{y}) \phi(\mathbf{y} + t\mathbf{u}, t) d\mathbf{y} dt. \end{aligned} \quad (\text{A.5})$$

A change back to the variable  $\mathbf{x}$  will result in Equation (A.2).

We now evaluate  $(\mathbf{u} - \mathbf{v}) \cdot \nabla \chi$ . To simplify, we set  $\mathbf{w} = \mathbf{u} - \mathbf{v}$ . We then have,

$$\langle \mathbf{w} \cdot \nabla \chi, \phi \rangle = - \int \chi(\mathbf{x}) \mathbf{w} \cdot \nabla \phi(\mathbf{x}) d\mathbf{x} = - \int_{\Omega} \mathbf{w} \cdot \nabla \phi(\mathbf{x}) d\mathbf{x}. \quad (\text{A.6})$$

Since  $\mathbf{w} \cdot \nabla \phi(\mathbf{x}) = \text{div } \mathbf{w} \phi(\mathbf{x})$ , we make use of Gauss' theorem in the plane to conclude that

$$\langle \mathbf{w} \cdot \nabla \chi, \phi \rangle = - \int_B \mathbf{w} \cdot \mathbf{N}(\mathbf{x}) \phi(\mathbf{x}) ds, \quad (\text{A.7})$$

where  $ds$  is the arc-length element of  $B$ .

Remembering that  $\delta(B(\mathbf{x}))$  is defined by the line integral [20]

$$\langle \delta(B(\mathbf{x})), \phi \rangle = \int_B \phi(\mathbf{x}) ds, \quad (\text{A.8})$$

we obtain

$$\langle \mathbf{w} \cdot \nabla \chi, \phi \rangle = - \langle \delta(B(\mathbf{x})), \mathbf{w} \cdot \mathbf{N} \phi \rangle = - \langle \mathbf{w} \cdot \mathbf{N} \delta(B(\mathbf{x})), \phi \rangle, \quad (\text{A.9})$$

and therefore

$$(\mathbf{u} - \mathbf{v}) \cdot \nabla \chi = -(\mathbf{u} - \mathbf{v}) \cdot \mathbf{N} \delta(B(\mathbf{x})). \quad (\text{A.10})$$

We finally obtain

$$\alpha(\mathbf{v})[\chi(\mathbf{x} - t\mathbf{u})] = -(\mathbf{u} - \mathbf{v}) \cdot \mathbf{N}(\mathbf{x} - t\mathbf{u}) \delta(B(\mathbf{x} - t\mathbf{u})). \quad (\text{A.11})$$